

# Harmonic Compensation with Zero Sequence Load Voltage Control in a Speed Sensorless DFIG Based Stand-alone VSCF Generating System

M. Pattnaik, *Member, IEEE* and D. Kastha, *Member, IEEE*

**Abstract** — Doubly Fed Induction Generator (DFIG) based stand-alone VSCF systems reported so far cannot supply nonlinear unbalanced load current containing co-phasor components. This paper presents three topologies of a stand-alone DFIG which can handle this type of load. The harmonic/unbalance component of the load current in each case is supplied by the stator side converter. In the first option a  $\Delta/Y$  transformer with neutral connection supplies the load. However, the harmonic current circulating in the delta winding still distorts the load phase voltage beyond the acceptable limit. As a solution the zero sequence load voltage is actively controlled through the stator side converter with the load neutral connected to the midpoint of the dc link capacitor. But this configuration also fails when the load current contains dc component as in half wave rectifiers. Finally, a configuration with an additional inverter leg connected to the load neutral is proposed in conjunction with the zero sequence stator voltage controller. Simulation and experimental results from this last configuration demonstrate its excellent load voltage regulation property while supplying various nonlinear and unbalanced loads. The control algorithm is implemented without any speed/ position sensor.

**Index Terms**— Doubly Fed Induction Generator (DFIG), Harmonic compensation, Model Reference Adaptive System (MRAS), Stand-alone VSCF generator, Sensorless control, Wind energy.

## NOMENCLATURE

### General

$v_{dq}^e, i_{dq}^e$  :  $d, q$ -axis stator side inverter voltage and current in the synchronously rotating ref. frame.  
 $v_{dqs}^e, i_{dqs}^e$  :  $d, q$ -axis stator voltage and current in the synchronously rotating ref. frame.  
 $v_{dqr}^e, i_{dqr}^e$  :  $d, q$ -axis rotor voltage and current in the synchronously rotating ref. frame.  
 $v_{dqr}^r, i_{dqr}^r$  :  $d, q$ -axis rotor voltage and current in the rotor ref. frame.  
 $|\bar{i}_r|$  : Magnitude of the rotor current space vector.  
 $Q_{ref}, Q_{esi}$  : Instantaneous and steady state rotor reactive power

$r_s, r_r'$  : Per phase stator and rotor resistances (stator referred).  
 $l_s, l_r'$  : Per phase stator, rotor self inductances (stator referred).  
 $l_m$  : Per phase magnetizing inductance.  
 $\sigma$  : Total leakage coefficient.  
 $l_{f,r_f}$  : Transformer inductance and effective resistance.  
 $C, c_f$  : DC link and filter capacitance.  
 $\omega_e$  : Rotational speed of the stator flux (elect. rad/sec).  
 $\omega_r$  : Rotor speed of the induction machine (elect. rad/sec).  
 $\omega_{sl}$  : Slip frequency (elect. rad/sec).  
 $\omega_h$  : Harmonic frequency (elect. rad/sec).

### Superscripts

$\wedge$  : Estimated value.  
 $*$  : Reference value.

## I. INTRODUCTION

Variable Speed Constant Frequency (VSCF) wind power generation using Doubly Fed Induction Generators (DFIG) has been very popular due to their reduced converter size and consequent economic advantages ([1], [2]). Operation of these systems under unbalanced grid condition has been extensively reported in literature [3]-[8]. Presently, similar interest is being shown towards stand-alone generators using this machine [9]-[23].

The economic advantage of the DFIG based VSCF wind power generation over other schemes, as elaborated in [1] and [2] can be extended to autonomous applications provided acceptable supply voltage quality while feeding all possible combinations of loads can be ensured. Majority of the research work (except [15], [21]) reported so far on this topic attempt to control the load voltage by manipulating the magnetizing component of the DFIG rotor current, making the response sluggish. To supply nonlinear/unbalanced loads, some of the reported work ([9], [10], [11], and [15]) inject harmonic current through the stator side converter, while others ([13], [14], [16]-[20]) use the rotor side converter. At the rated operating condition of the system (i.e. maximum speed and rated torque) both the rotor and the stator side converters as well as the machine operate at their respective rated currents. Therefore, if the rotor side converter is to be used for harmonic current injection, current rating of not just the converter but the machine current rating must also be increased. This will be disadvantageous for wind power applications since a larger machine has to be carried on the tower top. Besides, harmonic current flowing through the machine rotor will generate pulsating torque which will put additional stress on the wind turbine drive train components

Manuscript received October 1, 2012; revised November 21, 2012; accepted for publication December 2, 2012.

Copyright © 2012 IEEE. Personal use of this material is permitted. However, permission to use this material for any other purposes must be obtained from the IEEE by sending a request to pubs-permissions@ieee.org.

M. Pattnaik is with the Department of Electrical Engineering, National Institute of Technology, Rourkela 769008, India. (phone: +91-8093767792; fax: 0661-2472926; e-mail: monalisa.pattnaik@gmail.com).

D. Kastha is with the Department of Electrical Engineering, Indian Institute of Technology, Kharagpur 721302, India (e-mail: kastha@ee.iitkgp.ernet.in).

even if no mechanical resonance is induced. Moreover, zero sequence component of the load current cannot be compensated through the rotor side due to three wire connection. On the other hand, injecting harmonic current through the stator side converter, will increase its current rating but will avoid all the other problems mentioned so far since the injected harmonic current will bypass the machine. As will be seen later it can also be used to compensate the co-phasor component of the load current.

In any case, the algorithms reported so far extract the harmonic/unbalance component of the load voltage/current to generate the reference waveform for the compensating current. This process introduces a phase distortion in the required compensating current waveform. To synthesize the compensating current the converters are controlled either simultaneously in several rotating reference frames ([9]-[15]) where each reference frame generates the voltage command for a pair of harmonic components or in a single reference frame using specialized controllers ([16]-[20]), one each for a pair of harmonic components. Both the approaches make the control algorithm exceedingly complex for practical implementation when nonlinear unbalanced loads such as single phase diode rectifiers are considered. Not only does this load require a large number of low frequency harmonic currents to be compensated the narrow separation among them, also makes their extraction very difficult. Possibly for this reason, stand-alone DFIG supplying this type of load has not been reported till very recently. For the first time, a control algorithm for these generators was proposed in [21] to handle loads which are unbalanced as well as nonlinear. No special harmonic/unbalance compensation strategy or extraction of the load voltage/current harmonic components was necessary. A speed sensorless control strategy for this system was reported in [22], [23].

However, the system configuration proposed in [21] - [23] does not allow the flow of co-phasor load current. Nor, to the best of our knowledge, does any other literature reported so far address this problem in any depth. In this paper, three different modifications to the system proposed in [21], are presented so that the generator can operate with general nonlinear and unbalanced loads. First a  $\Delta/Y$  connected transformer is inserted at the output of the stator side converter. The star connected winding offered neutral connection to the load. The closed delta winding provided a low impedance path for the circulation of the reflected co-phasor current. However, with single phase nonlinear load the load phase voltage waveform was found (by simulation) to have unacceptable Total Harmonic Distortion (THD). Hence the system is further modified by removing the transformer and connecting the load neutral point to the midpoint of the dc link capacitor. A zero sequence load voltage controller is also implemented for active compensation of the co-phasor load current. This system operates satisfactorily with both 3-ph and 1-ph nonlinear loads, but fails when the load current contains dc component such as in a half wave rectifier. Therefore, in the final modification, the load neutral is connected to an

additional leg of the stator side converter (identical to other legs) to carry the co-phasor load current. The zero sequence load voltage controller is also retained. Simulation and experimental results verify that this system can supply all the above mentioned loads (and more) keeping the load voltage and stator current THD within acceptable limits.

## II. REACTIVE POWER BASED SPEED SENSORLESS CONTROL OF THE VSCF GENERATOR

In the DFIG based VSCF generator, described in [21], the load and the machine terminals are connected together at the output of an LC filter fed from the stator side converter. The load voltage is closed loop controlled through this stator side converter to emulate a "stiff grid". The two loop cascade stator voltage controller structure has the filter inductor current as the inner loop control variable. The harmonic/unbalance compensation performance of the system is largely determined by the bandwidth of this inner filter current control loop. The load voltage components are controlled in the outer loop. The references for the direct and quadrature axis load voltages are so determined as to maintain the machine stator flux and its rotational frequency constant respectively. Detailed analysis of the stator side converter controllers is presented in [21]. The quadrature axis rotor current controls the dc link voltage. Changing this current varies the machine torque and hence the mechanical power input to the system. The direct axis rotor current is used to control the stator side power factor of the machine. Detailed analysis of the rotor side converter and DC link voltage controllers is presented in [24]. All the controllers are designed in the stator flux oriented reference frame. The stator flux linkage and the unit vectors for field orientation are found by integrating the stator voltages. A similar control structure, but without the dc link voltage controller has also been proposed in [15].

A speed sensorless control algorithm is proposed for this system in [22] and [23]. This algorithm estimates the stator flux oriented rotor current components ( $\hat{i}_{qr}^e$  &  $\hat{i}_{dr}^e$ ) from the measured stator and rotor currents. It also transforms the rotor converter voltage commands generated by the rotor current controllers from the stator flux oriented reference frame to the rotor reference frame as shown in Fig.1.

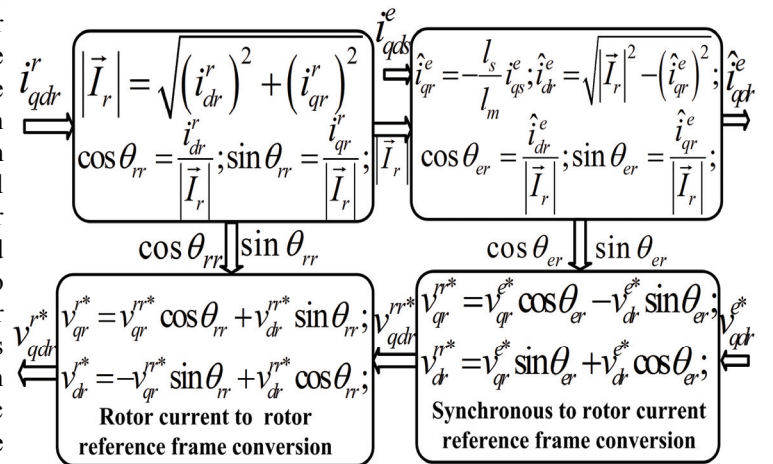


Fig.1. Block diagram for the reference frame conversion.

In the above block diagram  $\theta_{rr}$  and  $\theta_{er}$  are the angles the rotor current space vector makes with the  $d$ -axis of the rotor reference frame and the stator field oriented reference frame respectively. As the angle between the rotor current and the commanded rotor voltage space vectors is reference frame independent rotor position information is not required for these conversions. Only the slip speed information is used for back-emf compensation in the rotor current controllers. This slip speed is estimated using a reactive power based MRAS (Q-MRAS) observer shown in Fig.2. In this figure the symbol “ $\otimes$ ” represents “cross product between two vectors.

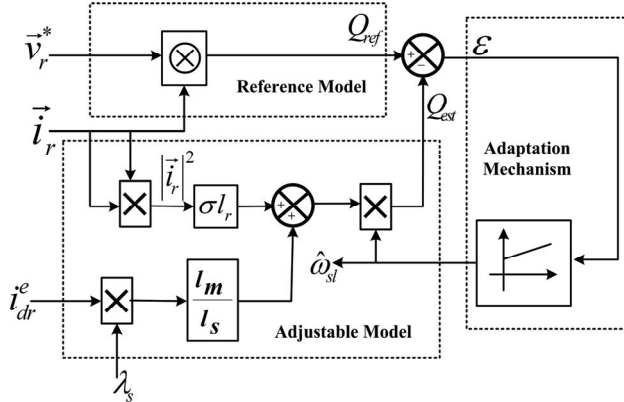


Fig. 2. Reactive power based MRAS observer.

A detailed analysis of the speed sensorless control algorithm as well as experimental verification can be found in [23]. The same speed sensorless control algorithm is used in all the configurations discussed subsequently in this paper.

### III. CO-PHASOR LOAD CURRENT COMPENSATION TECHNIQUES

#### A. System with a $\Delta/Y$ Transformer

As the system proposed in [21] does not allow the flow of co-phasor load currents (zero sequence fundamental components and triplen harmonic components) it is first modified by incorporating a  $\Delta/Y$  connected transformer at the output of the stator side converter as shown in Fig.3 (a).

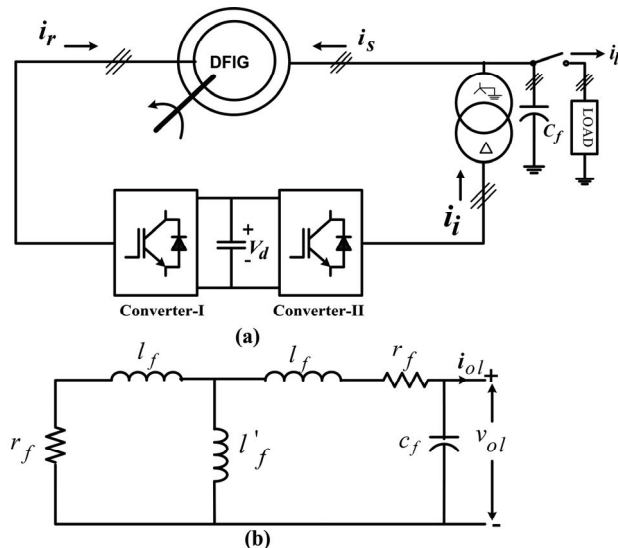


Fig.3. (a) Schematic diagram of the DFIG based VSCF system with a two winding transformer (b) its zero sequence equivalent circuit.

The  $o$ -axis equivalent circuit of the  $\Delta/Y$  connected transformer in the stator field oriented reference frame can be derived following the procedure in [25] and is shown in Fig.3(b). The inductance  $l_f'$  accounts for the zero sequence flux in the transformer core. In a 3 phase transformer with 3 limb core the zero sequence flux completes path through the transformer support structure (tank etc.). ‘ $l_f'$ ’, in that case, is negligibly small. Clearly the zero sequence equivalent circuit of the transformer forms a parallel resonant circuit with the filter capacitor. As a result, co-phasor component of the load phase voltage experiences “resonant amplification” at certain load harmonic frequencies. This is verified by simulating the system shown in Fig. 3(a) supplying a 2.0 kW single phase diode bridge rectifier load. Parameters of the power circuit components of Fig.3 are given in TABLE I.

TABLE I  
SPECIFICATIONS OF THE SYSTEM

Induction machine (stator referred)	
Stator (8 pole, $\nabla$ connected)	220 V, 50 Hz, 22 A (RMS)
Rotor (8 pole, Y connected)	300 V, 9 A (RMS)
Rated power / speed	5.6 kW / 720 RPM
Stator resistance/ phase ( $r_s$ )	0.87 $\Omega$
Rotor resistance/ phase ( $r_r'$ )	1.12 $\Omega$
Stator reactance/ phase ( $x_s$ )	12.4 $\Omega$
Rotor reactance/ phase ( $x_r'$ )	12.4 $\Omega$
Magnetizing reactance/ phase ( $x_m$ )	11.3 $\Omega$
Prime Mover (DC Machine)	
Armature winding: 220V, 35A ; Field winding: 220V, 1.7A	
Rated power output: 7.46 kW at 1500 RPM, 6.44 kW at 1300 RPM.	
Converter rating	
Stator side: 230V (RMS), 12A (RMS)	Rotor side: 230V (RMS), 9A (RMS)
$\Delta/Y$ transformer	
Rated Power	10 kVA
$\Delta$ -winding (stator side)	220V(L-L)
Y-winding (load)	220V(L-L)
Transformer parameters: $l_f$ : 0.93 mH, $r_f$ : 0.15 $\Omega$ ,	
Filter capacitor: $c_f$ : 100 $\mu$ F, 200 V, star connected	

In the simulation model the  $q$  and  $d$  axis components of the stator voltage controllers are similar to those described in [21]. However, due to three wire connection to the transformer  $\Delta$  winding zero sequence component of the load voltage cannot be controlled. The simulated waveform of the zero sequence load phase voltage and its frequency spectrum are shown in Fig. 4 (a) and (b) respectively. Resonance amplification of the zero sequence component of the load voltage at about 750 Hz is clearly visible from this figure. It should also be noted that successive harmonic components in the frequency spectrum of the zero sequence load phase voltage up to the resonance frequency do not attenuate appreciably although the zero sequence harmonic current amplitudes themselves decrease inversely proportional to their frequency.

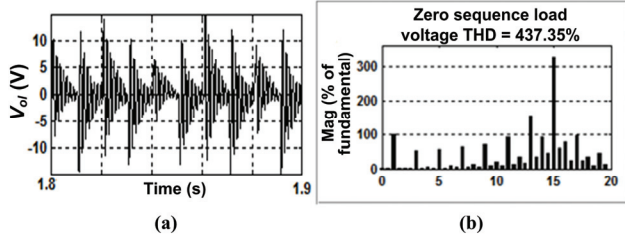


Fig.4. Simulated waveforms with the 2-winding transformer feeding 1-ph nonlinear load (a) load phase voltage zero sequence component, (b) DFT of load phase voltage zero sequence component.

This is understandable, since the zero sequence parallel resonant circuit (Fig. 3(b)) is predominantly inductive up to the resonance frequency. As a result of these two phenomena the THD of the load phase voltage is found to be 5.16 % which is above the acceptable limit.

### B. System with Split DC Link Capacitor

To handle nonlinear unbalanced loads more effectively another modification to the system is proposed by removing the transformer and connecting the load neutral to the midpoint of the dc link capacitor. The dc link capacitor is divided in to two series connected parts  $C_1$  and  $C_2$ , each of 4mF, 220 V, so that the equivalent dc link capacitance remains same (2 mF) as before. The schematic diagram of the modified system with split dc link capacitor is shown in Fig.5 (a). The  $d^e-q^e$  axis equivalent circuit of this modified stator side converter (along with the LC filter and load) remains the same as described in [21]. Consequently, the same stator voltage controllers as reported in [21] are also used in this case without any modification. However, a zero sequence equivalent circuit can now be drawn for the stator side converter arrangement shown in Fig.5 (a). This equivalent circuit and the proposed zero sequence stator voltage controller are shown in Fig.5 (b) & (c) respectively.

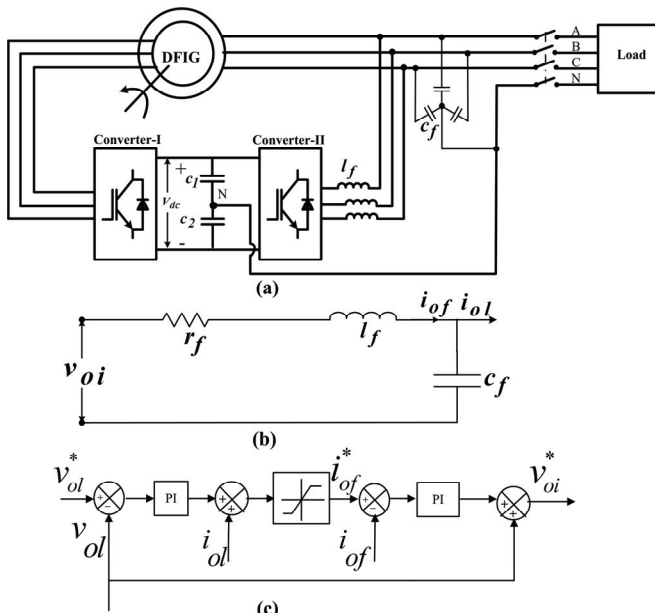


Fig.5. (a) block diagram with split dc link capacitor (b) zero sequence equivalent circuit, (c) controller block diagram for the zero sequence stator voltage controller.

In this figure  $v_{oi}$ ,  $v_{ol}$ ,  $i_{of}$  and  $i_{ol}$  refer to the zero sequence components of the inverter voltages, load voltages, filter currents and load currents respectively. The design of the PI controllers in this block diagram is the same as that of the  $d^e-q^e$  axis stator voltage and current controllers [21]. The output of this zero sequence controller is now used along with the outputs of the  $d^e-q^e$  axis voltage controllers to generate the modulating waves for the three stator side inverter phase legs.

This system is verified (by simulation) to perform satisfactorily for both balanced 3-ph and 1-ph (connected between a line and the neutral) diode bridge rectifier loads. However, when the system is subjected to a 420 W of 3- ph half wave diode rectifier load (connected between the three phases and the neutral) all the waveforms become highly distorted as shown in Fig. 6. Both the dc link capacitor voltages diverge (Fig. 6 (d)) due to the dc component of the neutral current. Obviously, this arrangement cannot handle such loads.

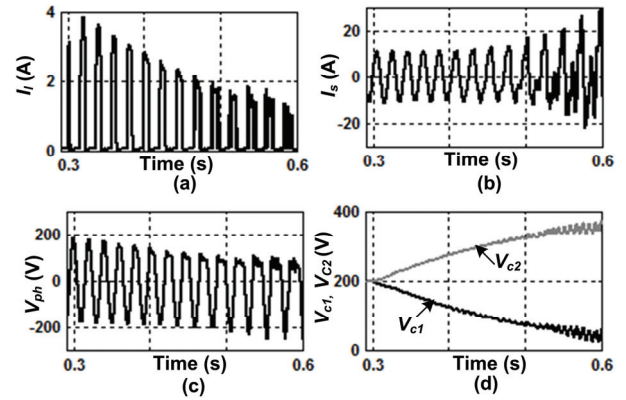


Fig.6. Simulated waveforms with the split dc link capacitor feeding 3-ph half bridge diode rectifier load (a) load current, (b) stator current, (c) load phase voltage, (d) charging & discharging of dc link voltage.

### C. System with Four Leg Inverter

In the third modification a fourth inverter leg identical to the other inverter legs is added to the stator side converter and connected to the neutral point of the load as shown in Fig. 7. The average output voltage at the fourth leg of the inverter is maintained at half the dc link voltage by PWM control with 50% duty cycle. The stator side voltage and the current controllers are also modified to add the zero sequence load voltage controller described in the previous section. This system is found to work satisfactorily with a 420 W of 3-ph half wave rectifier load feeding RL-load on the DC side as in the previous case. In addition, all the three configurations are also tested by simulation with 3 phase diode rectifier load, single phase linear and diode rectifier load as well as 3 phase half wave rectifier load (feeding RL load on the dc side). Performance of these systems under these loading conditions are summarized in TABLE II. From this table it is clear that only the last option (with 4 leg inverter) can handle all these types of loads with acceptable performance. Therefore, this configuration is chosen for experimental verification.

TABLE II  
HARMONIC COMPENSATION PERFORMANCE COMPARISON

Configuration	$\Delta/Y$ transformer (without zero sequence controller)		Split dc link capacitor (with zero sequence controller)		4 leg inverter (with zero sequence controller)	
	THD (%)	-ve sq / 0 sq (%)	THD (%)	-ve sq / 0 sq (%)	THD (%)	-ve sq / 0 sq (%)
3-ph full bridge rectifier R-load (4.3 kW)						
Phase voltage	2.92	0.0	2.25	0.0	1.98	0.0
Line voltage	2.80	0.0	2.25	0.0	2.04	0.0
Sator current	0.89	0.0	1.23	0.0	1.82	0.0
1-ph linear RL-load (2 kW)						
Phase voltage	0.0	0.45 / 0.77	0.0	0.57/2.82	0.0	0.41/0.96
Line voltage	0.0	0.49 / 0.0	0.0	0.49/0.0	0.0	0.45/0.0
Sator current	0.0	0.44 / 0.0	0.0	0.416/0.0	0.0	0.413/0.0
1-ph full bridge rectifier RL-load (2 kW)						
Phase voltage	<b>5.16</b>	0.57 / 0.80	2.43	0.565 / 2.94	2.25	0.56 / 1.02
Line voltage	3.82	0.65 / 0.0	1.59	0.49 / 0.0	2.25	0.65 / 0.0
Sator current	3.76	0.87 / 0.0	1.39	0.496/0.0	1.23	0.82 / 0.0
3-ph half bridge rectifier RL-load (420 W)						
Phase voltage	3.07	0.55/0.0	-	-	0.82	0.27 / 0.11
Line voltage	2.95	0.484/0.0	-	-	1.07	0.32 / 0.0
Sator current	<b>6.73</b>	0.465/0.0	-	-	1.40	0.36/ 0.0

At this point it will be pertinent to appreciate the economic implication of the choice. Compared to Fig.3 (a), the system proposed in Fig. 7 requires an additional inverter phase leg, its gate drive circuits and an additional voltage and current sensor. The output three phase transformer of Fig. 3(a) is also replaced by three air core line reactors of the same current rating. The price difference between a four leg inverter and a three leg inverter (both equipped with voltage and current sensors on the ac side) will generally, be higher than the price difference between the three phase transformer and the line reactors. For the present design, the four leg inverter system was costlier than the transformer based system by about 5% of the cost of the three leg inverter. Compared to Fig. 5(a) the system of Fig. 7 requires an additional inverter phase leg and its gate drivers but no additional sensors. However, the system of Fig. 5(a) required almost double the energy storage capacity at the DC link for handling the harmonic current flowing through them. For the present design, the system of Fig. 7 was costlier than the system in Fig. 5(a) by about 8% of the cost of the three leg inverter. Of course, the exact cost difference will be greatly influenced by the system voltage and power levels. In general, the split dc link capacitor based system will be more attractive economically, provided no dc component is expected in the neutral current. However, even in this case, the generally poor reliability record of electrolytic capacitors should be carefully compared against the additional cost of the fourth inverter leg for making the final choice.

#### IV. EXPERIMENTAL VERIFICATION OF THE FOUR LEG INVERTER

Block diagram of the laboratory proto type VSCF generator is shown in Fig.7.

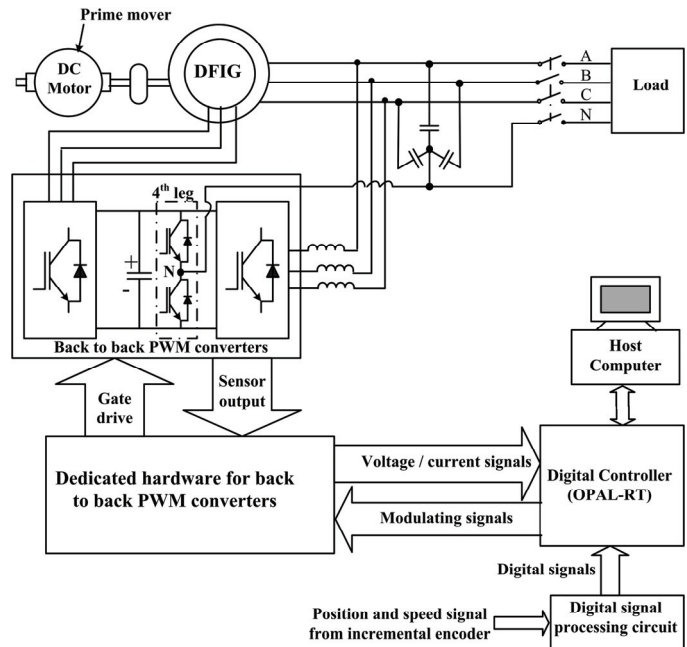


Fig.7. Block diagram of the DFIG based VSCF system with a 4 leg inverter.

The performance of the control algorithm with the zero sequence voltage controller and 4 leg inverter is tested experimentally. Specification of the major power circuit components are given in TABLE I. The speed sensorless control algorithm described in [22] and [23] with the added zero sequence voltage controller (Fig. 5 (c)) is implemented using RT-LAB real-time simulation platform from Opal-RT.

The system is first tested with the application of a 2.0 kW (36 % of m/c rating) 1-ph diode rectifier load between a line and the neutral at 3.31 sec. The load current waveform is shown in Fig. 8(a). At the load impact, the machine speed (Fig. 8(b)) drops from 980 r/min in the super-synchronous range to 710 r/min in the sub-synchronous range. The estimated rotor speed is seen to faithfully follow the actual rotor speed during the transient operation. Neither the machine stator flux nor the RMS load line voltage show any significant transient due to this load impact. Slight unbalance in the load phase voltage can be seen after loading in Fig. 8 (c). No other undesirable transients are observed in these waveforms. Fig. 8 (d) shows smooth transition of the rotor currents through the synchronous speed. Fig. 8(e) shows three phase machine stator currents which are sinusoidal without appreciable harmonic distortion. Harmonic and unbalance component of the load current is supplied completely from the stator side converter current (Fig. 8(f)). The waveforms and the DFT of the unbalanced nonlinear load current, load phase voltage and stator current under the above loading condition are shown in Fig.9. (a)-(f).

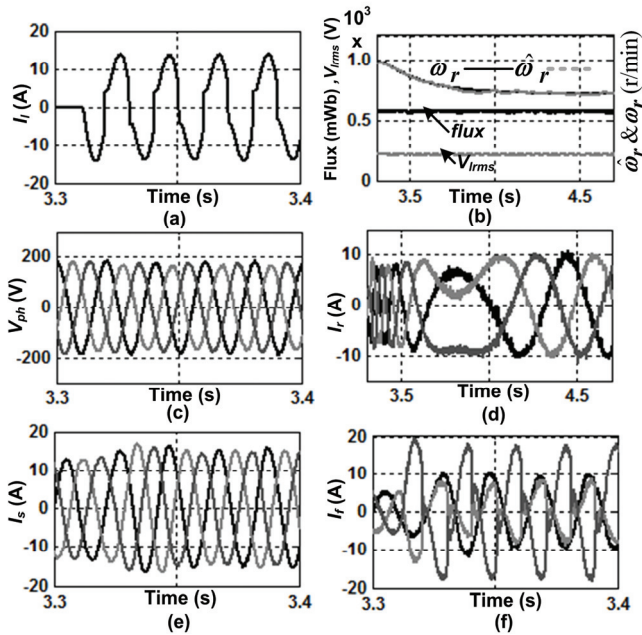


Fig. 8. Experimental transient waveforms of the system with 4 leg inverter feeding 2.0 kW 1-ph nonlinear load at sub-synchronous speed (a) load current, (b) rotor speed, stator flux and RMS load line voltage, (c) load phase voltage, (d) rotor current, (e) stator current, (f) filter current.

The negative sequence component of the stator current, load line voltage and load phase voltage are 2.62%, 1.75% and 1.72% of their fundamental positive sequence components respectively. The zero sequence component of the load phase voltage is 4.57 %.

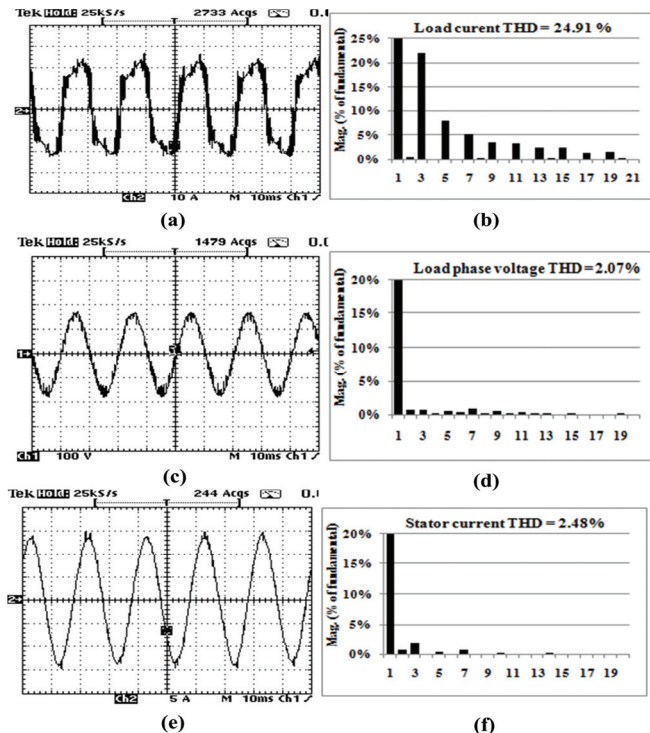


Fig. 9. Experimental steady state waveforms of the system with 4 leg inverter feeding 1-ph nonlinear load (a) load current, (b) DFT of load current, (c) load phase voltage, (d) DFT of load phase voltage, (e) stator current, (f) DFT of stator current.

Experimental evidence to sustained synchronous speed operation of a sensorless controlled DFIG is lacking in the reported literature. This is verified in Fig. 10 with the application of a 1.6 kW 3-ph diode bridge rectifier load.

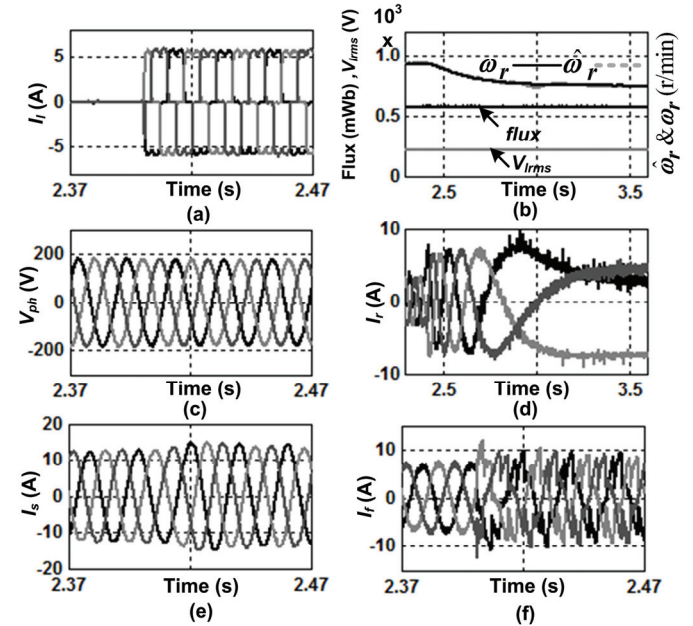


Fig. 10. Experimental waveforms of the system with 4 leg inverter feeding 1.6kW 3-ph nonlinear load at synchronous speed (a) load current, (b) actual and estimated rotor speed, stator flux and RMS load line voltage, (c) 3-ph load phase voltage, (d) 3-ph rotor current, (e) 3-ph stator current, (f) 3-ph filter current.

Fig. 10(b) shows that after loading the machine speed settles down to the synchronous value (750 r/min) with the estimated speed faithfully tracking the actual machine speed all the time. Consequently, the rotor current waveforms shown in Fig. 10(d) become ‘dc’ after loading. However, other variables such as RMS line voltage, machine flux (Fig. 10 (b)), the load phase voltages (Fig. 10(c)), the stator line currents (Fig. 10(e)) show no undesirable transient / harmonic distortion, confirming satisfactorily sustained operation at the synchronous speed. The nonlinear load current (Fig. 10 (a)) is supplied completely from the stator side converter (Fig. 10(f)).

In a wind power generation application the loading of the system can be significantly increased at increased machine speed. Therefore, the system is next tested with the application of a 4.3 kW (77 % of the machine rating) 3-ph nonlinear (3-ph diode bridge rectifier) load at 2.23 sec. One of the load phase current waveform is shown in Fig. 11 (a). Even with such a large load step, load phase (Fig. 11 (b)) or line voltage (Fig. 11(d)) do not show any significant transient disturbance proving the effectiveness of the stator voltage controller. All the currents i.e. stator line current (Fig. 11 (a)), stator side inverter line current (Fig. 11 (a)), and the rotor and the rotor side inverter line currents (Fig. 11 (c)) increase substantially to support the additional load but remain well within their respective current ratings as given in TABLE I. As before, the estimated rotor speed is found to track the actual machine speed (Fig. 11 (d)) with negligible error.

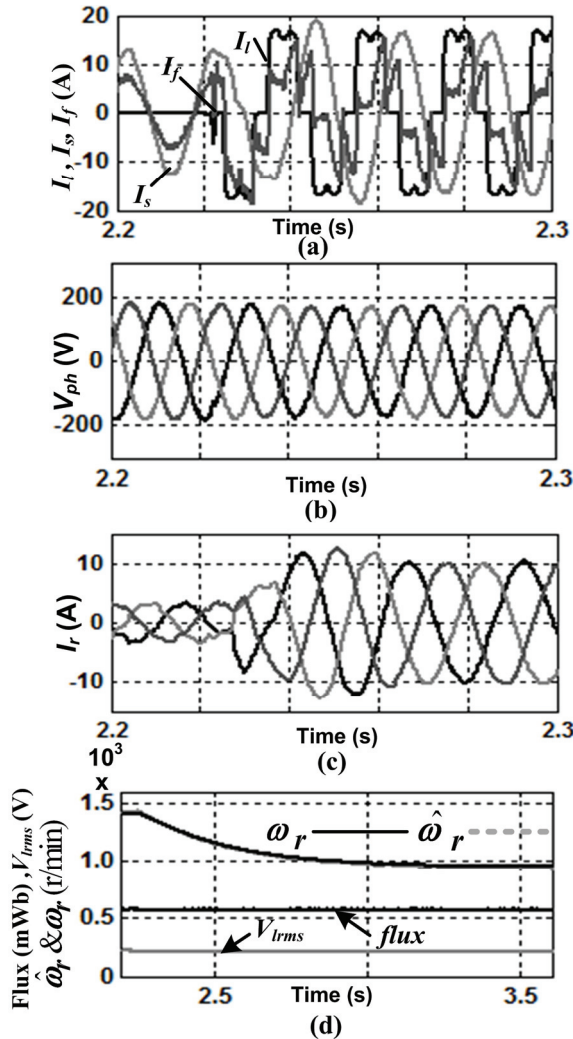


Fig.11. Experimental transient waveforms of the system with 4 leg inverter feeding 4.3 kW 3-ph nonlinear load at super-synchronous speed (a) inverter, stator and load current, (b) load phase voltage, (c) rotor current, (d) actual and estimated rotor speed, stator flux and RMS load line voltage.

The waveforms and the DFT of the 3-ph nonlinear load current, load phase voltage and stator current are shown in Fig.12. (a)-(f). The system is also tested with 420 W of 3-ph half wave rectifier load. The experimental waveforms and the DFT of the load current, load phase voltage and stator current are shown in Fig.13. (a)-(h). The operating speed of the machine in this case is 1100 r/min.

TABLE III summarizes the performance of the system in terms of THD and sequence components (whenever applicable) of different system variables for different types of loads. In this table the THD data are expressed in terms of percentage of the fundamental component while the sequence component data are expressed in terms of the percentage of the positive sequence fundamental component of the corresponding variable. Both experimental and simulation results are shown with experimental results in bold font. Clearly, the proposed system can restrict the load voltage and stator current THD and sequence components within acceptable limits for a very wide variety of loading conditions.

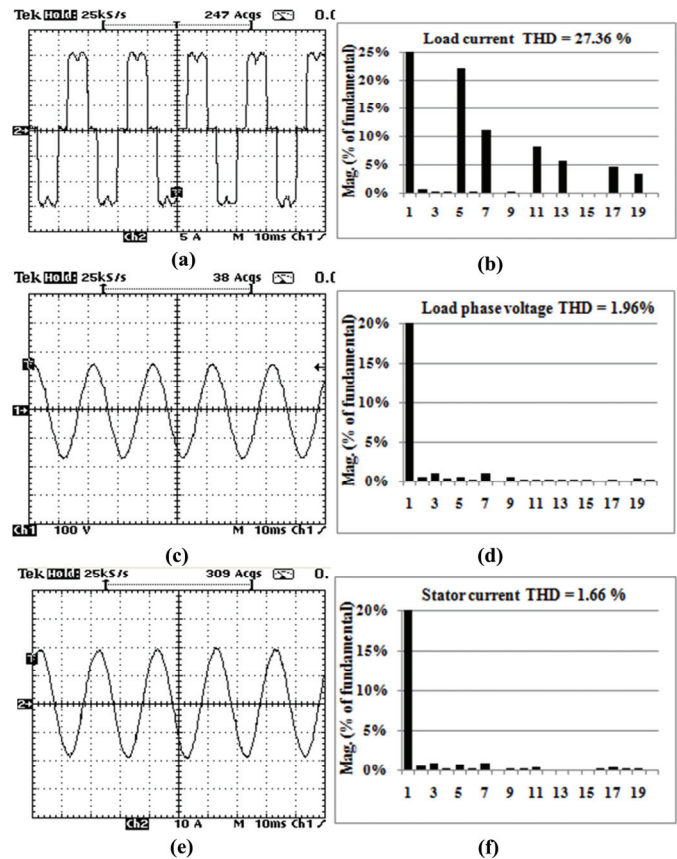


Fig.12. Experimental steady state waveforms of the system feeding 4.3 kW 3-ph nonlinear load (a) load current, (b) DFT of load current, (c) load phase voltage, (d) DFT of load phase voltage, (e) stator current, (f) DFT of stator current.

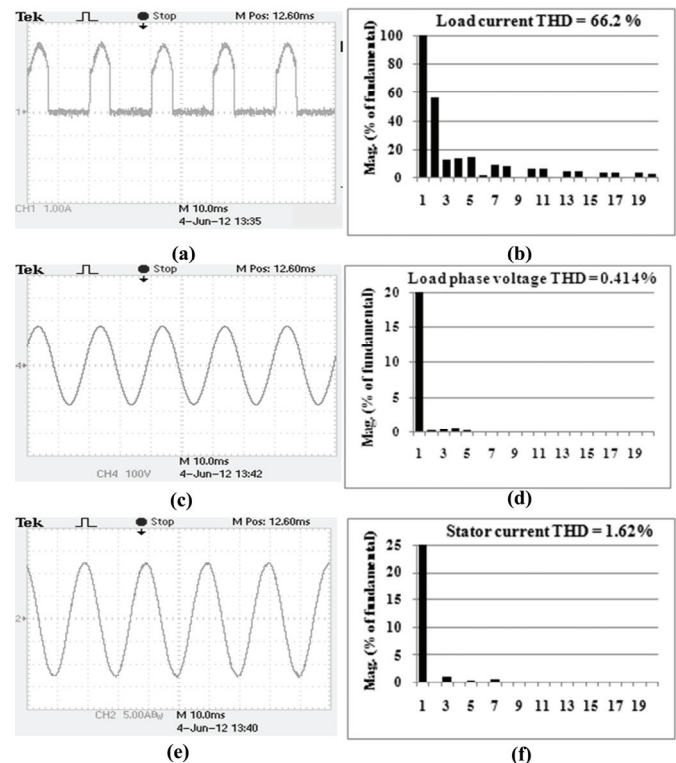


Fig.13. Experimental waveforms of the system with 4 leg inverter feeding 3-ph half bridge rectifier load (a) load current, (b) DFT of load current, (c) load phase voltage, (d) DFT of load phase voltage, (e) stator current, (f) DFT of stator current.

TABLE III  
PERFORMANCE WITH FOUR LEG INVERTER

Variable	Stator current		Load line voltage		Load phase voltage		
	THD (%)	-ve sq (%)	THD (%)	-ve sq (%)	THD (%)	-ve sq (%)	o-sq (%)
Load condition							
3-ph diode rectifier R-L load (4.3 kW)	1.66	0.0	2.4	0.0	1.96	0.0	0.0
3-ph diode rectifier R-C load (1 kW)	2.38	0.0	2.84	0.0	3.15	0.0	0.0
1-ph linear load (2 kW)	-	2.37	0.0	1.56	-	1.57	4.05
1-ph diode rectifier R-L load (2 kW)	2.48	2.62	1.61	1.75	2.07	1.72	4.57
2-ph linear, 1-ph nonlinear load (2.8 kW)	1.57	1.18	1.96	0.31	1.27	0.314	0.31
2-ph nonlinear, 1-ph linear load (2.8 kW)	1.55	1.2	1.26	0.47	1.55	0.47	1.02
3-ph half wave diode rectifier R-L load (420W)	1.62	0.95	0.42	0.29	0.41	0.29	0.17

It is observed that in some cases (2<sup>nd</sup>, 3<sup>rd</sup> and 4<sup>th</sup> row) mismatch between simulated and experimental data exist. A closer observation revealed that the PWM modulator of the stator side converter was saturating in parts of the cycle, specially at the peak of the filter current waveforms, with these loads and hence the compensation was not perfect. This may have been caused by the additional voltage drop in the semiconductor devices and connecting cables as well as due to the “dead time” between the switches in a phase leg. Moreover, in the experimental system the stator current also carried harmonics of the magnetization current due to machine saturation. None of these effects were modeled in simulation.

Finally Fig. 14 shows variable speed operation of the proposed generation system. In, Fig.14 (a), (b) and (c) the machine speed changed from 1050 r/min to 650 r/min and back in 1.6 sec with the system operating at no load. For Fig.14 (d), (e) and (f) the speed change is from 1080 r/min to 530 r/min and back in 1.7 sec. In this case the system is supplying 1.8 kW of resistive load. In both cases acceleration and deceleration is in excess of 500 rpm/sec. Fig.14 (a) & (d) shows that the estimated speed tracks the actual speed with only marginal (less than 5 r/min) error. Even such a rapid change in the rotor speed has no effect on either the common dc bus voltage or the load line voltage (Fig.14 (b) & (e)) which demonstrates the effectiveness of the dc link voltage controller and the stator voltage controllers. In both cases 50 % of the magnetizing current is supplied from the rotor side converter. The torque components of the rotor current in both the cases are comparatively smaller at high speed (about 1050 r/min). Hence, the rotor currents (Fig.14 (c) & (f)) have almost identical magnitude in both the cases at high speed. However, as the speed decreases the torque component of the rotor current increases rapidly to supply the connected load in the second case. Therefore, the rotor current at the minimum speed in Fig.14 (f) is much large compared to Fig.14 (c).

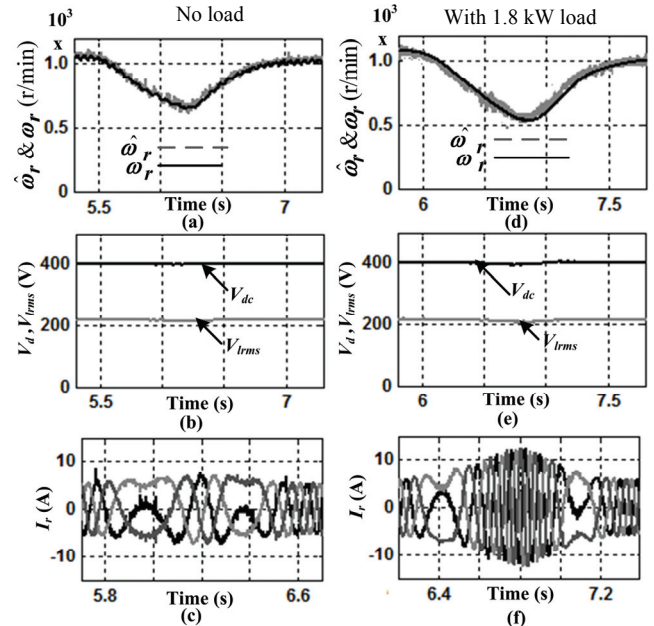


Fig.14. Experimental results during speed transient (a),(d) actual and estimated rotor speed, (b),(e) DC link voltage and RMS load voltage, (c),(f) rotor currents.

## V. CONCLUSION

This paper investigates the performance of a speed sensorless DFIG based stand-alone VSCF generator feeding general nonlinear unbalanced loads. Three different modifications to the basic DFIG system are proposed out of which it is found that the system with  $\Delta/Y$  connected transformer works well with balanced 3 phase nonlinear load and single phase linear load but not with single phase nonlinear load. On the other hand a system with a split dc link capacitor to connect the load neutral (and no transformer) works well with both 3-ph and single phase nonlinear loads but fails completely if the load neutral current contains dc component. Finally, a system with a four leg stator side converter is found suitable (by simulation and experiment) for all types of loads that may be expected in a stand-alone application. The system also regulates the load voltage tightly during severe load and speed transients. The speed observer works satisfactorily under all operating conditions. Therefore, it can be concluded that if only linear loads (balanced or unbalanced) are to be supplied the system with two winding transformer will suffice. However, if the load is expected to be both unbalanced and nonlinear then one of the last two configurations must be chosen depending on whether or not the load neutral current may contain dc component.

## REFERENCES

- [1] M. Liserre, R. Cárdenas, M. Molinas, and J. Rodríguez, “Overview of multi-MW wind turbines and wind parks,” *IEEE Trans. Ind. Electron.*, vol. 58, no. 4, pp. 1081-1094, Apr. 2011.
- [2] H. Polinder, F. F. A. van der Pijl, G.-J. de Vilder, and P. Tavner, “Comparison of direct-drive and geared generator concepts for wind turbines,” *IEEE Trans. Energy Convers.*, vol. 21, no.3, pp. 725- 733, Sept. 2006.

- [3] X. Lie and W. Yi, "Dynamic modeling and control of DFIG-based wind turbines under unbalanced network conditions," *IEEE Trans. Power Syst.*, vol. 22, no.1, pp. 314-323, Feb. 2007.
- [4] Y. Jun, L. Hui, L. Yong, and C. Zhe, "An improved control strategy of limiting the dc-link voltage fluctuation for a doubly fed induction generator," *IEEE Trans. Power Electron.*, vol. 23, no.3, pp. 1205-1213, May 2008.
- [5] J. Hu and Y. He, "Modeling and enhanced control of DFIG under unbalanced grid voltage conditions," *Electr. Power Syst. Res.*, vol. 79, no.2, pp. 273-281, Feb. 2009.
- [6] G. Abad, M. A. Rodriguez, G. Iwanski, and J. Poza, "Direct power control of doubly-fed-induction-generator-based wind turbines under unbalanced grid voltage," *IEEE Trans. Power Electron.*, vol. 25, no.2, pp. 442-452, Feb. 2010.
- [7] L. Fan, H. Yin, and Z. Miao, "A novel control scheme for DFIG-based wind energy systems under unbalanced grid conditions," *Electr. Power Syst. Res.*, vol. 81, no.2, pp. 254-262, Feb. 2011.
- [8] N. Heng, S. Yipeng, Z. Peng, and H. Yikang, "Improved direct power control of a wind turbine driven doubly fed induction generator during ransient grid voltage unbalance," *IEEE Trans. Energy Convers.*, vol. 26, no.3, pp. 976-986, Sept. 2011.
- [9] A. K. Jain and V. T. Ranganathan, "Wound rotor induction generator with sensorless control and integrated active filter for feeding nonlinear loads in a stand-alone grid," *IEEE Trans. Ind. Electron.*, vol. 55, no.1, pp. 218-228, Jan. 2008.
- [10] R. Pena, R. Cardenas, E. Escobar, J. Clare, and P. Wheeler, "Control system for unbalanced operation of stand-alone doubly fed induction generators," *IEEE Trans. Energy Convers.*, vol. 22, no.2, pp. 544-545, Jun. 2007.
- [11] R. Pena, R. Cardenas, E. Escobar, J. Clare, P. Wheeler, "Control strategy for a doubly-fed induction generator feeding an unbalanced grid or stand-alone load," *Electr. Power Syst. Res.*, vol. 79, no. 2, pp. 355-364, Feb. 2009.
- [12] R. Cardenas, R. Pena, J. Clare, G. Asher, and J. Proboste, "MRAS observers for sensorless control of doubly-fed induction generators," *IEEE Trans. Power Electron.*, vol. 23, no.3, pp. 1075-1084, May 2008.
- [13] G. Iwanski and W. Koczara, "Sensorless direct voltage control of the stand-alone slip-ring induction generator," *IEEE Trans. Ind. Electron.*, vol. 54, no.2, pp. 1237-1239, Apr. 2007.
- [14] G. Iwanski and W. Koczara, "DFIG based power generation system with UPS function for variable speed application," *IEEE Trans. Ind. Electron.*, vol.55, no. 8, pp. 3047-3054, Aug. 2008.
- [15] T. Bhattacharya and L. Umanand, "Negative sequence compensation within fundamental positive sequence reference frame for a stiff micro-grid generation in a wind power system using slip ring induction machine," *IET Electr. Power Appl.*, vol. 3, no.6, pp. 520-530, Nov. 2009.
- [16] V.-T. Phan and H.-H. Lee, "Improved predictive current control for unbalanced stand-alone doubly-fed induction generator-based wind power systems," *IET Electr. Power Appl.*, vol. 5, no.3, pp. 275-287, Mar. 2011.
- [17] V.-T. Phan, K. Sung-Hyo, and H.-H. Lee, "An improved control method for DFIG-based wind system supplying unbalanced stand-alone loads," *IEEE International Sympo. Ind. Electron.*, pp. 1081-1086, Jul. 2009.
- [18] V.-T. Phan and H.-H. Lee, "Stationary frame control scheme for a stand-alone doubly fed induction generator system with effective harmonic voltages rejection," *IET Electr. Power Appl.*, vol. 5, no.9, pp. 697-707, Nov. 2011.
- [19] V.-T. Phan and H.-H. Lee, "Control strategy for harmonic elimination in stand-alone DFIG applications with nonlinear loads," *IEEE Trans. Power Electron.*, vol. 26, no.9, pp. 2662-2675, Sept. 2011.
- [20] V.-T. Phan and H.-H. Lee, "Performance enhancement of stand-alone DFIG systems with control of rotor and load side converters using resonant controllers," *IEEE Trans. Ind. Appl.*, vol. 48, no.1, pp. 199-210, Jan./Feb.2012.
- [21] M. Pattnaik and D. Kastha, "Control of double output induction machine based stand-alone variable speed constant frequency generator with nonlinear and unbalanced loads," *IEEE PES General Meeting 2010*, Minneapolis, Minnesota, USA, pp.1-8, Jul. 2010.
- [22] M. Pattnaik and D. Kastha, "Reactive power based MRAS observer for speed sensorless control of double output induction generator," *ICIIIS 2010*, NIT Surathkal, India, pp.556-561, Jul./Aug. 2010.
- [23] M. Pattnaik and D. Kastha, "Adaptive speed observer for a stand-alone doubly fed induction generator feeding nonlinear and unbalanced loads," *IEEE Trans. Energy Convers.*, vol. 27, no. 4, pp.1018-1026, Dec. 2012.
- [24] Isha T.B. and D. Kastha, "Transient performance of a stand-alone variable speed constant frequency generation system," *Power Conversion Conference-Nagoya*, Japan, pp. 622-628, Apr.2007.
- [25] P. C. Krause, O. Wasynczuk, and S. D. Sudoff, "Analysis of electric machinery and drive systems," IEEE press and Wiley Interscience, N. J. 2004.

## BIOGRAPHIES



**Monalisa Pattnaik** (S'11-M'12) received the B.Tech. degree in Electrical Engineering from College of Engineering and Technology, OUAT, Bhubaneswar, Odisha, India, in 1999 and the M. Tech. degree in Machine Drives and Power Electronics from Indian Institute of Technology Kharagpur, India, in 2006 and she is pursuing the Ph.D. degree at Indian Institute of Technology, Kharagpur. She was working in the department of Electrical Engineering, Institute of Technical Education and Research, SOAU, Bhubaneswar, Odisha from June 2002 to July 2008. She is currently an Assistant Professor in the Department of Electrical Engineering, NIT Rourkela, Odisha, India. Her research area is Machine Drives and Power Electronics.



**Debaprasad Kastha** (M'94) received the B.E. degree in Electrical Engineering from Bengal Engineering College, Calcutta University, India, in 1987, the M.E. degree in electrical engineering from Indian Institute of Science, Bangalore in 1989 and the Ph.D. degree from the University of Tennessee, Knoxville, in 1994.

From March 1989 to December 1989 he worked in the Research and Development (Electronics) Division, Crompton Greaves, Ltd, Bombay, India. He joined the Department of Electrical Engineering, Indian Institute of Technology, Kharagpur, India as a lecturer in April 1994, became Assistant Professor in Jan. 1996. Presently he holds the post of Professor. His research interest includes Wind Energy, Machine Drives and Power Electronics.